


Phonon-mediated superconductivity in the metal-bonded perovskite Al_4H up to 54 K under ambient pressure

Yong He, Jing Lu, Xinqiang Wang, and Jun-jie Shi ^{*}

State Key Laboratory for Artificial Microstructures and Mesoscopic Physics, School of Physics, Peking University Yangtze Delta Institute of Optoelectronics, Peking University, Beijing 100871, China



(Received 8 August 2022; revised 14 June 2023; accepted 2 August 2023; published 17 August 2023)

Multihydrogen lanthanum hydrides have shown the highest critical temperature T_c at 250–260 K under pressures of 170–200 GPa. However, such high pressure is a great challenge for sample preparation and practical applications. To address this challenge, we propose a design strategy for ambient-pressure superconductors that involves constructing few-hydrogen metal-bonded perovskite hydrides, such as the Al-based superconductor Al_4H , with better ductility than the well-known multihydrogen, cuprate, and Fe-based superconductors. Based on the Migdal-Eliashberg theory, we predict that the structurally stable Al_4H has a favorable T_c of up to 54 K under ambient pressure.

DOI: [10.1103/PhysRevB.108.054515](https://doi.org/10.1103/PhysRevB.108.054515)

I. INTRODUCTION

Hydrogen, the lightest element with the smallest radius, has been predicted to possess the highest superconducting transition temperature $T_c \sim 356$ K with a metallic modification at an ultrahigh pressure near 500 GPa [1,2]. Unfortunately, experimental observation of this T_c for metallic hydrogen has not yet been confirmed even at about 400 GPa [3,4]. In 2004, Ashcroft suggested that hydrogen-dominant materials, i.e., multihydrogen hydrides, could be powerful candidates for high- T_c superconductors under moderate pressure, where the combination of hydrogen and other elements can produce chemical precompression to reduce the pressure of hydrogen metallization [5]. Following this idea, many multihydrogen covalent hydrides have been predicted by using structural search methods at high pressure, and some of them have been synthesized by using a diamond anvil cell [6]. Duan *et al.* predicted that $(\text{H}_2\text{S})_2\text{H}_2$ with $Im\bar{3}m$ structure possesses a high T_c of 191–204 K under a pressure of 200 GPa [7], which was confirmed by experiments [8]. A number of multihydrogen materials, such as SiH_4 [9], YH_9 [10], LaH_{10} [11,12], ThH_{10} [13], and CaH_6 [14], have been synthesized successively, and their superconductivity with T_c 's of about 17, 243, 250–260, 161, and 215 K, respectively, has been certified under high pressure. The superconductivity of Th_4H_{15} and $(\text{Th}M_x)_4\text{H}_{15}$ ($M = \text{Ce, La, Zr, Bi, Y}$) was observed at $T_c \sim 8.05$ – 8.35 and $T_c \leq 7.5$ K at ambient pressure [15] and 50 atm [16], respectively. Based on first-principles simulations, Vocaturo *et al.* predicted that PdCuH_2 is a superconductor with $T_c \sim 34$ K at ambient pressure [17]. The estimated T_c in CrH (CrH_3) is 10.6 (~ 37.1) K at atmospheric pressure (81 GPa) [18]. As a high-temperature superconductor, KB_2H_8 is predicted with $T_c \sim 134$ – 146 K around 12 GPa [19].

Among multihydrogen materials, aluminum hydrides have been recognized as important hydrogen storage and

superconducting materials. As one of the most promising hydrogen storage materials, AlH_3 has been extensively studied due to its high amount of hydrogen storage and rapid dehydrogenation capacity [20]. The calculated T_c in AlH_3 , a poor superconductor due to the absence of conduction electrons caused by Al^{+3} and H^{-1} , rapidly decreases with compression and becomes less than 2.04 K at 110 GPa [21,22], and it eventually approaches zero at above 210 GPa [23], as confirmed by experiments [24]. The superconductivity of AlH_2 with $T_c = 6.75$ K, dominated by the electron–optical-phonon coupling [25], has been observed in experiments [26]. The calculated T_c of AlH with $R\bar{3}m$ symmetry is about 58 K under a pressure of 180 GPa, and the estimated T_c of Al_2H with $P\bar{3}m1$ structure is 3.5 K at 195 GPa [23]. Obviously, the superconductivity of few-hydrogen aluminum hydrides is still absent under ambient pressure.

Considering that both the face-centered cubic (fcc) and body-centered cubic (bcc) lattices are very common metal crystal structures and thoroughly analyzing the relationship [see Eq. (1)] between fcc, bcc, and perovskite structures,

$$\text{fcc} + \text{bcc} \xrightarrow{\text{vertex sharing}} \text{perovskite}, \quad (1)$$

we propose the idea of constructing a few-hydrogen metal-bonded perovskite hydride derived from a fcc metal with the smallest-radius H atom at its body center as an ambient-pressure superconductor, different from the semiconducting and metallic perovskites featuring ionic and covalent bonds; this idea can be regarded as a complete reversal of the conventional design strategy of multihydrogen high- T_c superconductors at several hundred GPa, which is impractical. Because aluminum is the only material with good ductility, low density, ultrahigh abundance, and environmental friendliness for long-distance power transmission, it would bring great benefits to humanity if it became a practical superconductor. As an application of our idea, the binary Al-based metal-bonded perovskite Al_4H is chosen, in which the body-centered H atom, occupying the “sphere interstice” of the

^{*}Corresponding author: jjshi@pku.edu.cn

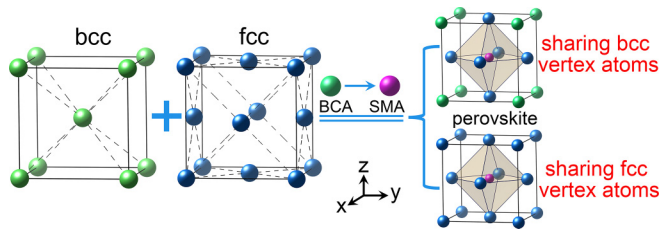


FIG. 1. The design idea for few-hydrogen metal-bonded perovskites, formed by combining a bcc metal lattice—with the body-centered atom (BCA) replaced by a small-mass atom (SMA) or small-radius atom—and a fcc metal lattice, with a much larger packing fraction than a fcc lattice. At top right, a ternary perovskite (see Table S3 for several examples) is depicted, derived from the bcc and fcc lattices by sharing bcc vertex atoms. If sharing fcc vertex atoms, a binary perovskite (shown at bottom right) can be obtained. The fcc body center, i.e., the octahedral interstice O_h , can be regarded as a normal lattice point from the viewpoint of perovskite. If the body center of a fcc metal, such as aluminum, is occupied by a H atom, which is the lightest element with the smallest radius, a typical binary Al-based metal-bonded perovskite, Al_4H , can be formed naturally.

Al atom lattice, is naturally fixed by the stable fcc skeleton of Al atoms without any extrinsic pressure. The electronic band structure, phonon dispersion, electron-phonon coupling (EPC), and superconducting properties have been investigated theoretically. Excellent superconducting characteristics and ductility of Al_4H are confirmed at ambient pressure, which is favorable for motivating experimental investigations and even practical applications in the future.

II. RESULTS AND DISCUSSION

A. Design idea and crystal structure

Because many metals adopt fcc and bcc structures, we thus theoretically design few-hydrogen metal-bonded perovskite hydrides to realize superconductivity at ambient pressure. Our idea is illustrated in Fig. 1; the left side of the figure shows the bcc conventional cell, with six intrinsic vacancies at its face centers, and the fcc conventional cell, with a natural vacancy at its body center. Comparing fcc structures with bcc structures, the body center of the fcc structure can easily be occupied by a small-radius atom, such as a H, He, or B atom, to form a metal-bonded perovskite structure (two such structures are shown at right in Fig. 1). Naturally, we choose a H atom to occupy the body center of fcc aluminum, an environment-friendly and low-cost superconductor with $T_c \sim 1.20$ K [27], to form perovskite Al_4H (see Table S1 and Fig. S4 of the Supplemental Material [28] for its lattice constant, Wyckoff position, Bader charge, and x-ray diffraction pattern [29]). Obviously, two key issues, closely related to multihydrogen high- T_c superconductors, i.e., ultrahigh pressure and poor ductility caused by the covalent bond, can be solved by our designed few-hydrogen metal-bonded perovskites under ambient pressure.

B. Structural stability

Considering that the structural stability of perovskite Al_4H is the foundation of its superconductivity, we thus comprehensively check its stability based on the crystal

structure, the formation energy, *ab initio* molecular dynamics (AIMD) simulations, phonon spectra, and previous experiments for hydrogen implantation in fcc aluminum with two highly competitive interstitial sites, i.e., octahedral (O_h) and tetrahedral (T_d) [26,30–46] (see Secs. SII and SIII, Figs. S1, S2, and S5–S8, and Table S2 of the Supplemental Material [28]). From an experimental point of view, hydrogen implantation and diffusion in fcc aluminum, with two natural interstitial sites O_h and T_d occupied by the smallest-radius H atom, have been investigated previously. By means of the low-temperature hydrogen implantation method, Bugeat and co-workers realized effective hydrogen implantation in aluminum at 10 and 150 keV at 25–400 K and studied lattice localization and trapping of H atoms [35,36]. Hydrogen diffusion measurements were performed by applying potentiostatic and galvanostatic permeation and the current pulse method using the electrochemical double cell technique [37]. Hydrogen diffusion is also investigated by analyzing the kinetic behavior predicted for solutions of hydrogen in aluminum [38] and by the desorption method [39]. Wei *et al.* proved that H atoms can be introduced into thin crystalline aluminum films at 10–20 K with overall long-range order and the fcc Al lattice is always stable even if the atomic ratio of H to Al is about 1 : 1 [34]. Moreover, Lamoise *et al.* reported that H atoms can be implanted into aluminum thin films with implantation energy of 10 keV at temperatures below 6 K at a high average H-to-Al ratio up to 2 : 1 by using the Orsay ion implanter [26]. Hashimoto and Kino also performed an effective hydrogen implantation in aluminum crystals by gas phase charging in the temperature range 300–400 °C and by electrochemical charging at room temperature [40]. As stated above, H atoms can be implanted into fcc aluminum with a high atomic ratio of H to Al of about 2 : 1. The stability of the fcc Al lattice implanted by H atoms, occupying the interstitial site O_h or T_d , has been confirmed by many previous experiments [26,35–41]. This clearly indicates that perovskite Al_4H with a H atom at the O_h site, due to its lower energy than the T_d site (see Fig. S8 and Table S2), is the most stable phase under the conditions of a fcc Al lattice and an easily realized low H concentration of H : Al = 1 : 4, much lower than the H : Al = 2 : 1 that has been reported in experiments [26].

Based on the structural characteristics of Al_4H , the aforementioned theoretical analyses about its stability, and the experimental hydrogen implantation in fcc aluminum crystals, we can suggest five potential experimental synthesis schemes to prepare perovskite Al_4H in two steps, i.e., (1) hydrogen implantation and (2) hydrogen diffusion in fcc aluminum crystals. Firstly, H atoms can be implanted into aluminum by using the low-temperature hydrogen implantation method as adopted previously [26]. Secondly, H atoms can also be introduced into aluminum by gas phase charging of H atoms under ambient pressure at 300 °C [40]. Thirdly, by means of electrochemical charging at room temperature [40], H atoms can also be implanted into fcc aluminum. Fourthly, Al_4H may also be synthesized via a direct reaction of aluminum and hydrogen at high pressure, i.e., pressure-driven formation, in which H atoms are pressed into aluminum, similar to the synthesis of lanthanum hydrides [11]. After H atoms are implanted into aluminum by using the above methods, both the O_h and T_d sites will be occupied by H atoms. Considering the

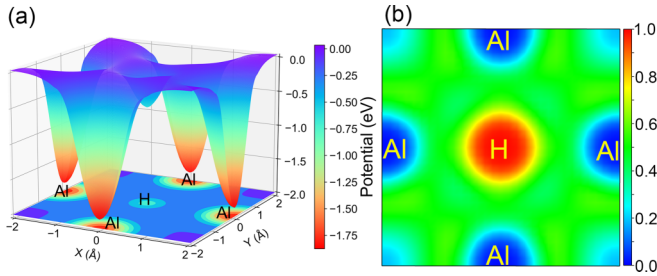


FIG. 2. Calculated electrostatic potential (a) and electron localization function (b) on the Al-H plane.

low energy barrier (0.09 eV) for H atom migration from the T_d site to the O_h site and the lowest energy of the O_h site (Fig. S8 and Table S2) and considering AIMD simulations (Figs. S6 and S7), we can confirm that H atoms prefer to occupy O_h sites. Therefore we can expect that H atoms at T_d sites may overcome the low energy barrier and migrate to O_h sites in the fcc Al lattice to form the favorable perovskite Al_4H under ambient pressure and at room temperature after a period of time, for example, 2 weeks [11]. Finally, we can expect that perovskite Al_4H viewed along the [111] direction, equivalent to an ultrashort-period $(Al_4)_1H_1$ superlattice, can also be controllably prepared directly on Al substrate by taking the following steps: performing plasma-assisted molecular beam epitaxy (MBE) with a k-cell source to steam Al and a hydrogen plasma source to steam H; accurately controlling the H-to-Al ratio in the excess-hydrogen environment; adjusting the substrate temperature at low temperature, for example, the liquid-nitrogen or liquid-helium temperature; and using the submonolayer digital-alloying technique [47].

Figure 2(a) shows the electrostatic potential on the Al-H plane in Al_4H , indicating that the H atom stays stably at the bottom of its potential well. After optimizing the crystal structure and calculating the zero-point energy by using several advanced functionals including the Perdew-Burke-Ernzerhof functional revised for solids (PBEsol) [32] and the Armiento-Mattsson 2005 functional (AM05) [45], we find that the body center O_h has the lowest energy, clarifying the long-running debate as to the priority of O_h and T_d sites for H atom occupation in aluminum [36,38,44,48]. The stability of perovskite Al_4H was further confirmed by using the DISORDER code with the enumeration method (Fig. S5) [49]. We believe from our careful calculations that few-hydrogen binary metal-bonded perovskite Al_4H with the H atom at the O_h site is the most stable structure under the preconditions of fcc aluminum and Al : H = 4 : 1.

C. Metallic binding and electronic structure

To clarify the nature of chemical bonds in Al_4H , we further investigate its electron localization function [Fig. 2(b)], i.e., the normalized electron density, which intuitively shows the bond characteristics between Al and H atoms. We find that both Al and H ions are immersed in an almost uniform electron sea with a normalized electron density of 0.6, indicating a typical metallic bond combination, different from multihydrogen covalent superconductors at high pressure. Obviously, these conduction electrons are mainly derived from 3s and 3p valence electrons of Al atoms. It is the Al-H metallic bond

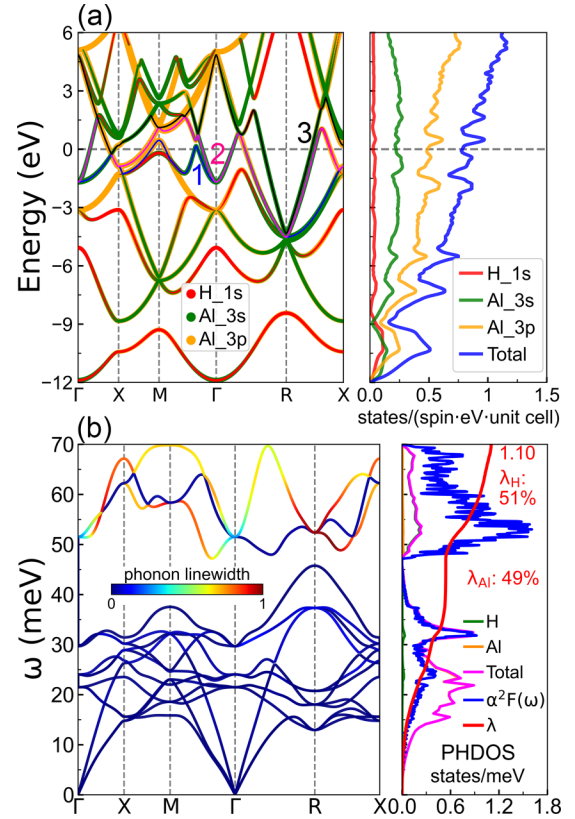


FIG. 3. Energy bands and corresponding projected DOS (a) and lattice dynamic properties (b) of Al_4H . In (a), the size of the colored circles shows the orbital character, which is proportional to the weight for the orbital contribution. In (b), the left panel shows the phonon spectra decorated with the normalized phonon linewidth, while the right panel shows the projected phonon DOS (PHDOS), Eliashberg spectral function $\alpha^2F(\omega)$, and EPC constant $\lambda = \lambda_{Al} + \lambda_H$.

that enhances the structural stability of Al_4H and guarantees its having better ductility than the multihydrogen, cuprate, and Fe-based superconductors.

Let us now investigate electronic structure of Al_4H . Figure 3(a) shows our calculated electronic bands with the resolved atomic orbital contribution [32,50–53], indicating a typical metal energy band with three bands, labeled as bands 1, 2, and 3, crossing the Fermi level ($E_F = 0$ eV). Figure S2(a) gives the corresponding Wannier interpolation bands. Band 1 is mainly dominated by Al 3s and 3p orbitals, consistent with Figs. S10(d) and S10(g), and has three camel shapes crossing E_F , one along the X - M - Γ direction, one along the M - Γ direction, and one along the Γ - R direction. Band 2 crosses E_F along the whole high-symmetry path. These multiple crossings at E_F give birth to a complex Fermi surface (FS) sheet, and the orbital characteristics can be derived from H 1s, Al 3s, and Al 3p states, in good agreement with Figs. S10(b), S10(e), and S10(h). Band 3, dominated by Al 3s and 3p orbitals [see Figs. S10(f) and S10(i)], is also shown near the Fermi level. We can deduce from the projected density of states (DOS) in the right panel of Fig. 3(a) that the 3s and 3p orbitals of Al atoms contribute almost 31.7 and 64.5% to the total DOS, while the contribution from the H 1s orbital is about 3.8%. It

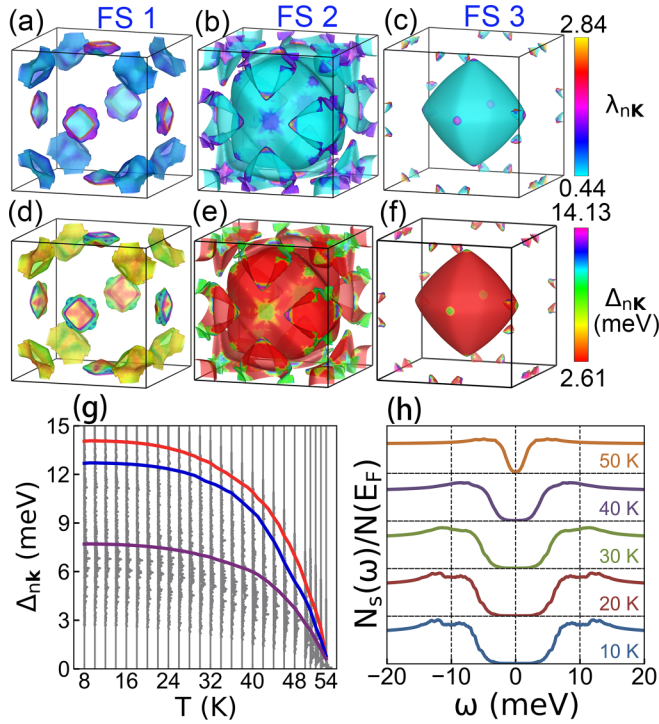


FIG. 4. EPC constant and superconducting gap of Al_4H . [(a)–(c)] Fully \mathbf{k} -resolved EPC strength $\lambda_{n\mathbf{k}}$ on the FS for the three crossing bands, bands 1, 2, and 3 [Fig. 3(a)]. [(d)–(f)] Fully \mathbf{k} -resolved superconducting gap $\Delta_{n\mathbf{k}}$ on the three FS sheets at 10 K. (g) The anisotropic superconducting gap $\Delta_{n\mathbf{k}}$ as a function of temperature, where the red, blue, and purple lines represent the gaps defined by the maximum normalized quasiparticle DOS. (h) The normalized quasiparticle DOS from 10 to 50 K.

is the three FS sheets induced by the three bands crossing E_F that dominate the three distinct superconducting gaps in Al_4H [Figs. 4(d)–4(g)] [54].

D. Phonon spectra and electron-phonon coupling

Before investigating the superconductivity, we carefully assess the anharmonic effects of Al_4H in Sec. SIV of the Supplemental Material [28] and find from Figs. S8 and S9 that Al_4H only exhibits weak anharmonicity [55–60]. We thus calculate the harmonic phonon spectra and EPC parameters of Al_4H by using density-functional perturbation theory [61] and Wannier interpolation technology on very fine \mathbf{q} and \mathbf{k} grids, as implemented in the EPW code [62–65]. Figure 3(b) shows the phonon spectra embellished with the phonon linewidth, phonon DOS (PHDOS), Eliashberg spectral function $\alpha^2F(\omega)$, and EPC strength λ determined by the phonon linewidth, closely related to the electron-phonon interaction matrix element describing the scattering probability amplitude of an electron on the FS by a phonon with wave vector \mathbf{q} [66]. The phonon spectra calculated using several different pseudopotentials including the optimized norm-conserving Vanderbilt pseudopotential (ONCV) [53], the ultrasoft pseudopotential (USPP), and the projector augmented wave method (PAW) [67] are comprehensively compared with the all-electron spectra [68] (Fig. S1). The commonly used acoustic sum rules,

such as “simple” and “crystal,” are also carefully checked. We can find from Figs. 3(b) and S2(b) that the phonon spectra are divided into two parts separated by a small phonon energy gap. The high-frequency (low-frequency) modes are dominated by H (Al) atom vibration. Compared with the maximum frequency of aluminum [69], the cutoff frequency of Al_4H has an increase of 60% due to vibration of the H atom with the lightest mass $m_H \sim m_{\text{Al}}/27$, which is highly desirable to improve T_c . The resolved phonon linewidth of all branches below 46 meV indicates that they have a similar EPC strength, except the mode around 31 meV with a slightly larger phonon linewidth. Compared with the low-frequency acoustic modes, the H-related high-frequency optical phonons have a much stronger EPC because of their large phonon linewidths.

We further investigate the Eliashberg spectral function $\alpha^2F(\omega)$ using the maximally localized Wannier function interpolation technology and accumulate the EPC constant λ [right panel of Fig. 3(b)]. The $\alpha^2F(\omega)$ exhibits a peak centered at 31 meV and a much larger main peak around 52 meV, which reveals great EPC due to the large phonon linewidth. The cumulative $\lambda = \lambda_{\text{Al}} + \lambda_{\text{H}}$ is 1.10, in which contributions from Al and H atoms are 49 and 51%, respectively. We find that λ in Al_4H is almost three times larger than that of aluminum (0.36) [69], and superior to MgB_2 (0.75) [70], because of the large phonon linewidth of the high-frequency H-vibration modes and slight softening of the low-frequency Al-vibration modes.

It is worthwhile to note that, as the source of all the properties of the Al-based superconductor Al_4H of interest here, the H atom has a larger λ_{H} than λ_{Al} , approaching 51% of the total EPC constant [Fig. 3(b)]. The key role of the H atom in the superconductivity of Al_4H can be analyzed as follows. Although the body-centered H atom, with a lower energy level than the Fermi level [Fig. 3(a)] and a much larger electronegativity than that of the Al atoms, takes electrons from its neighboring Al atoms to be localized around it [Fig. 2(b) and Table S1], the superconductivity of Al_4H is slightly affected by this electron transfer finally because the total DOS on the FS decreases very little from 0.82 states/[spin · eV · (unit cell)] in Al to 0.78 states/[spin · eV · (unit cell)] in Al_4H . In contrast, the H atom in Al_4H induces high-frequency optical phonons and greatly modifies the phonon spectra of aluminum [Fig. 3(b)]. Most importantly, these H-related high-frequency optical phonons have the largest phonon linewidth among all phonons, directly leading to a larger EPC constant λ_{H} than λ_{Al} due to strong EPC between the H-related phonon and the conduction electron [71]. This is extremely important to enhance the T_c of Al_4H , indeed [72]. Notably, a similar physical mechanism has also been found in graphite-intercalation compounds in which nonsuperconducting graphite presents a T_c of 12 K with Ca intercalation [73,74]. This rapid increase in superconductivity can be explained in terms of the contribution of local-phonon vibrations of lightly intercalated atoms. It is the large λ_{H} together with λ_{Al} that dominates the high T_c in Al_4H .

To evaluate the anisotropy of the EPC strength in Al_4H , we explored the \mathbf{k} -resolved EPC constant $\lambda_{n\mathbf{k}}$ defined by $\lambda_{n\mathbf{k}} = \sum_{m\mathbf{k}',v} \frac{1}{\omega_{qv}} \delta(\epsilon_{m\mathbf{k}'}) |g_{n\mathbf{k},m\mathbf{k}'}^v|^2$ [70]. Figures 4(a)–4(c) show the variation of $\lambda_{n\mathbf{k}}$ on the three FS sheets. The values of $\lambda_{n\mathbf{k}}$ on FSs 1, 2, and 3 have the wide ranges 0.45–2.84, 0.45–2.44,

and 0.44–1.00, respectively, indicating strong anisotropy inside each single sheet. Figure S11 also plots the normalized distribution of λ_{nk} with the wide range 0.45–2.84, further revealing strong anisotropy. We find that λ_{nk} on FS 1 is larger than that on FSs 2 and 3. Particularly, six flakes at the face centers of FS 1 exhibit the largest EPC strength because of the strong coupling of Al $3s$ and $3p$ electrons with phonons (Fig. S10). The EPC constant λ_{nk} mainly comes from H $1s$ and Al $3p$ orbitals. In contrast, FS 3, dominated by the Al $3s$ state, has the smallest contribution to λ_{nk} among the three FS sheets.

E. Superconducting gap and critical temperature

Furthermore, the superconducting gap Δ_{nk} of Al_4H has also been calculated on the FS by numerically solving the anisotropic Migdal-Eliashberg equations with $\mu^* = 0.1$ [70,75,76]. In Figs. 4(d)–4(f), we show the \mathbf{k} -resolved superconducting gap at 10 K on the three FS sheets. The gaps on FSs 1, 2, and 3 are in the ranges 2.61–14.13, 2.67–13.90, and 2.64–7.70 meV, respectively, indicating the strong anisotropy of Δ_{nk} on each single FS sheet with a large vertical energy spread [Figs. 4(g) and S3]. The larger the superconducting gap Δ_{nk} , the higher the critical temperature T_c . It is interesting to note that the distribution of Δ_{nk} is very similar to that of λ_{nk} , suggesting that Al_4H is a phonon-mediated superconductor.

Figure 4(g) presents the superconducting gap Δ_{nk} as a function of temperature, in which three fully anisotropic superconducting gaps originating from the three FS sheets are featured with a remarkable vertical energy spread, different from aluminum, which has a single gap [77,78]. The red, blue, and purple lines show the gaps corresponding to the maximum superconducting DOS on FSs 1, 2, and 3 [Fig. 4(h)], respectively. The three superconducting gaps belong to different FS sheets and always overlap with each other due to their large vertical energy spread and strong anisotropic EPC [Figs. 4(a)–4(c) and S10]. As temperature increases, the superconducting gaps decrease and eventually disappear at $T_c = 54$ K (51 K with $\mu^* = 0.13$; Fig. S12); this T_c is approximately 45 times higher than that of aluminum (1.20 K) [27], and higher than those of Nb_3Ge (23 K) [79] and MgB_2 (39 K) [80]. We further obtain $T_c = 42$ K from the isotropic Migdal-Eliashberg equations with $\mu^* = 0.10$. Obviously, both the anisotropic effect and multiband gaps, closely related to the strong anisotropy of EPC, greatly enlarge T_c , by about 28.6%, which shows that the anisotropic effect is very important to improve T_c , as confirmed by Ref. [54]. We also find that the average value of the three anisotropic single gaps is close to the isotropic single gap at $T \rightarrow 0$ K.

Moreover, we calculate the normalized quasiparticle DOS $N_S(\omega)$ at different temperatures based on the formula $\frac{N_S(\omega)}{N(E_F)} = \text{Re}[\frac{\omega}{\sqrt{\omega^2 - \Delta^2(\omega)}}]$ [70], where $N(E_F)$ represents the DOS of the normal state at the Fermi level. We can see from Fig. 4(h) that the superconducting gap decreases if the temperature increases. The normalized quasiparticle DOS, as a function of excitation energy, exhibits three peaks, closely related to three different energy gaps in Al_4H . Furthermore, to prove that our idea (Fig. 1) is fruitful, we find that, besides Al_4H , several other binary and ternary few-hydrogen metal-bonded perovskite $M_4\text{H}$ ($M = \text{Ca}, \text{Cu}, \text{Rh}$) and AHM_3 ($A = \text{V}, \text{Nb}; M = \text{Al}, \text{Rh}, \text{Ca}$) hydrides are also phonon-mediated superconductors under ambient pressure (Table S3). Finally, the specific heat and critical magnetic field are investigated (Fig. S13) [27,70,75,81–83].

III. CONCLUSION

In summary, we proposed an idea and found a class of materials named the few-hydrogen metal-bonded perovskite hydrides, such as the Al-based superconductor Al_4H , to be strong anisotropic phonon-mediated superconductors at ambient pressure, by combining first-principles calculations and the Wannier interpolation method and solving the Migdal-Eliashberg equations. The structural stability of Al_4H is confirmed. As an environmentally friendly and low-cost material, Al_4H , featuring metallic bonds, is a superconductor with both better ductility than multihydrogen, cuprate, and Fe-based superconductors combined by covalent and ionic bonds and a T_c of up to 54 K. Therefore, contrary to the conventional design method of multihydrogen covalent high- T_c superconductors at high pressure, our idea paves the way for designing few-hydrogen metal-bonded hydride superconductors with a simple structure under ambient pressure. We hope that this study will rekindle enthusiasm for predicting new materials with favorable superconducting properties among hydrides at ambient pressure and can stimulate further experimental investigation in the near future.

ACKNOWLEDGMENTS

This work was supported by the Beijing Outstanding Young Scientist Program (Grant No. BJJWZYJH0120191000103) and the National Natural Science Foundation of China (Grants No. 61734001 and No. 61521004). We used the High Performance Computing Platform of the Center for Life Science of Peking University.

- [1] N. W. Ashcroft, Metallic Hydrogen: A High-Temperature Superconductor? *Phys. Rev. Lett.* **21**, 1748 (1968).
- [2] J. M. McMahon and D. M. Ceperley, High-temperature superconductivity in atomic metallic hydrogen, *Phys. Rev. B* **84**, 144515 (2011).
- [3] B. Monserrat, N. D. Drummond, P. Dalladay-Simpson, R. T. Howie, P. López Ríos, E. Gregoryanz, C. J. Pickard, and R. J. Needs, Structure and Metallicity of Phase V of Hydrogen, *Phys. Rev. Lett.* **120**, 255701 (2018).

- [4] P. Loubeyre, F. Occelli, and P. Dumas, Synchrotron infrared spectroscopic evidence of the probable transition to metal hydrogen, *Nature (London)* **577**, 631 (2020).
- [5] N. W. Ashcroft, Hydrogen Dominant Metallic Alloys: High Temperature Superconductors? *Phys. Rev. Lett.* **92**, 187002 (2004).
- [6] J. A. Flores-Livas, L. Boeri, A. Sanna, G. Profeta, R. Arita, and M. Eremets, A perspective on conventional high-temperature

- superconductors at high pressure: Methods and materials, *Phys. Rep.* **856**, 1 (2020).
- [7] D. Duan, Y. Liu, F. Tian, D. Li, X. Huang, Z. Zhao, H. Yu, B. Liu, W. Tian, and T. Cui, Pressure-induced metallization of dense $(\text{H}_2\text{S})_2\text{H}_2$ with high- T_c superconductivity, *Sci. Rep.* **4**, 6968 (2014).
- [8] A. P. Drozdov, M. I. Eremets, I. A. Troyan, V. Ksenofontov, and S. I. Shylin, Conventional superconductivity at 203 kelvin at high pressures in the sulfur hydride system, *Nature (London)* **525**, 73 (2015).
- [9] M. I. Eremets, I. A. Trojan, S. A. Medvedev, J. S. Tse, and Y. Yao, Superconductivity in hydrogen dominant materials: Silane, *Science* **319**, 1506 (2008).
- [10] P. Kong, V. S. Minkov, M. A. Kuzovnikov, A. P. Drozdov, S. P. Besedin, S. Mozaffari, L. Balicas, F. F. Balakirev, V. B. Prakapenka, S. Chariton, D. A. Knyazev, E. Greenberg, and M. I. Eremets, Superconductivity up to 243 K in the yttrium-hydrogen system under high pressure, *Nat. Commun.* **12**, 5075 (2021).
- [11] A. P. Drozdov, P. P. Kong, V. S. Minkov, S. P. Besedin, M. A. Kuzovnikov, S. Mozaffari, L. Balicas, F. F. Balakirev, D. E. Graf, V. B. Prakapenka, E. Greenberg, D. A. Knyazev, M. Tkacz, and M. I. Eremets, Superconductivity at 250 K in lanthanum hydride under high pressures, *Nature (London)* **569**, 528 (2019).
- [12] M. Somayazulu, M. Ahart, A. K. Mishra, Z. M. Geballe, M. Baldini, Y. Meng, V. V. Struzhkin, and R. J. Hemley, Evidence for Superconductivity above 260 K in Lanthanum Superhydride at Megabar Pressures, *Phys. Rev. Lett.* **122**, 027001 (2019).
- [13] D. V. Semenok, A. G. Kvashnin, A. G. Ivanova, V. Svitlyk, V. Y. Fominski, A. V. Sadakov, O. A. Sobolevskiy, V. M. Pudalov, I. A. Troyan, and A. R. Oganov, Superconductivity at 161 K in thorium hydride ThH_{10} : Synthesis and properties, *Mater. Today* **33**, 36 (2020).
- [14] L. Ma, K. Wang, Y. Xie, X. Yang, Y. Wang, M. Zhou, H. Liu, X. Yu, Y. Zhao, H. Wang, G. Liu, and Y. Ma, High-Temperature Superconducting Phase in Clathrate Calcium Hydride CaH_6 up to 215 K at a Pressure of 172 GPa, *Phys. Rev. Lett.* **128**, 167001 (2022); **129**, 269901(E) (2022).
- [15] C. B. Satterthwaite and I. L. Toepke, Superconductivity of Hydrides and Deuterides of Thorium, *Phys. Rev. Lett.* **25**, 741 (1970).
- [16] H. Oesterreicher, J. Clinton, and M. Misroch, Studies of hydride formation and superconductivity in hydrides of alloys Th-M ($M = \text{La, Y, Ce, Zr}$ and Bi), *J. Less-Common Met.* **52**, 129 (1977).
- [17] R. Vocaturo, C. Tresca, G. Ghiringhelli, and G. Profeta, Prediction of ambient-pressure superconductivity in ternary hydride PdCuH_x , *J. Appl. Phys.* **131**, 033903 (2022).
- [18] S. Yu, X. Jia, G. Frapper, D. Li, A. R. Oganov, Q. Zeng, and L. Zhang, Pressure-driven formation and stabilization of superconductive chromium hydrides, *Sci. Rep.* **5**, 17764 (2015).
- [19] M. Gao, X.-W. Yan, Z.-Y. Lu, and T. Xiang, Phonon-mediated high-temperature superconductivity in the ternary borohydride KB_2H_8 under pressure near 12 GPa, *Phys. Rev. B* **104**, L100504 (2021).
- [20] M. Yu, Z. Zhu, H. P. Li, and Q. L. Yan, Advanced preparation and processing techniques for high energy fuel AlH_3 , *Chem. Eng. J.* **421**, 129753 (2021).
- [21] Y. K. Wei, N. N. Ge, G. F. Ji, X. R. Chen, L. C. Cai, S. Q. Zhou, and D. Q. Wei, Elastic, superconducting, and thermodynamic properties of the cubic metallic phase of AlH_3 via first-principles calculations, *J. Appl. Phys.* **114**, 114905 (2013).
- [22] A. K. M. A. Islam, M. M. Ali, and M. L. Ali, AlH_3 between 65 and 110 GPa: Implications of electronic band and phonon structures, *Phys. C (Amsterdam)* **470**, 403 (2010).
- [23] K. Abe, *Ab initio* study of metallic aluminum hydrides at high pressures, *Phys. Rev. B* **100**, 174105 (2019).
- [24] I. Goncharenko, M. I. Eremets, M. Hanfland, J. S. Tse, M. Amboage, Y. Yao, and I. A. Trojan, Pressure-Induced Hydrogen-Dominant Metallic State in Aluminum Hydride, *Phys. Rev. Lett.* **100**, 045504 (2008).
- [25] L. X. Wei and M. Gupta, Electron-phonon coupling and superconductivity of hydrogen implanted aluminium, *J. Less-Common Met.* **130**, 123 (1987).
- [26] A. Lamoise, J. Chaumont, F. Meunier, and H. Bernas, Superconducting properties of aluminium thin films after ion implantation at liquid helium temperatures, *J. Phys. Lett.* **36**, 271 (1975).
- [27] J. F. Cochran and D. E. Mapother, Superconducting transition in aluminum, *Phys. Rev.* **111**, 132 (1958).
- [28] See Supplemental Material at <http://link.aps.org/supplemental/10.1103/PhysRevB.108.054515> for a discussion of computational methods, structural stability, the priority of the octahedral and tetrahedral sites for hydrogen occupation in aluminium, anharmonic effects, electronic and superconducting properties, specific heat, and the critical magnetic field, which includes Refs. [26,27,29–46,48–53,55–65,67,68,70,75,76,81–83].
- [29] K. Momma and F. Izumi, *VESTA3* for three-dimensional visualization of crystal, volumetric and morphology data, *J. Appl. Crystallogr.* **44**, 1272 (2011).
- [30] G. Kresse and J. Furthmüller, Efficient iterative schemes for *ab initio* total-energy calculations using a plane-wave basis set, *Phys. Rev. B* **54**, 11169 (1996).
- [31] P. E. Blöchl, Projector augmented-wave method, *Phys. Rev. B* **50**, 17953 (1994).
- [32] J. P. Perdew, A. Ruzsinszky, G. I. Csonka, O. A. Vydrov, G. E. Scuseria, L. A. Constantin, X. Zhou, and K. Burke, Restoring the Density-Gradient Expansion for Exchange in Solids and Surfaces, *Phys. Rev. Lett.* **100**, 136406 (2008).
- [33] S. Nosé, Constant temperature molecular dynamics methods, *Prog. Theor. Phys. Suppl.* **103**, 1 (1991).
- [34] L. X. Wei, M. Ruault, A. Traverse, and H. Bernas, *In situ* electron microscopy study of implanted AlH_x , *J. Less-Common Met.* **130**, 133 (1987).
- [35] J. Bugeat, A. Chami, and E. Ligeon, A study of hydrogen implanted in aluminium, *Phys. Lett. A* **58**, 127 (1976).
- [36] J. Bugeat and E. Ligeon, Lattice location and trapping of hydrogen implanted in FCC metals, *Phys. Lett. A* **71**, 93 (1979).
- [37] H.-J. Schlüter, H. Züchner, R. Braun, and H. Buhl, Diffusion of hydrogen in aluminium, *Z. Phys. Chem.* **181**, 103 (1993).
- [38] R. B. McLellan, Hydrogen diffusion in aluminum, *Scr. Metall.* **17**, 1237 (1983).
- [39] K. Papp and E. Kovács-Csetényi, Diffusion of hydrogen in solid aluminium, *Scr. Metall.* **11**, 921 (1977).
- [40] E. Hashimoto and T. Kino, Hydrogen diffusion in aluminium at high temperatures, *J. Phys. F: Met. Phys.* **13**, 1157 (1983).

- [41] R. Ambat and E. S. Dwarakadasa, Effect of hydrogen in aluminium and aluminium alloys: A review, *Bull. Mater. Sci.* **19**, 103 (1996).
- [42] R. L. Mills and A. F. Schuch, Crystal Structure of Normal Hydrogen at Low Temperatures, *Phys. Rev. Lett.* **15**, 722 (1965).
- [43] J. P. Perdew, K. Burke, and M. Ernzerhof, Generalized Gradient Approximation Made Simple, *Phys. Rev. Lett.* **77**, 3865 (1996).
- [44] C. Wolverton, V. Ozoliņš, and M. Asta, Hydrogen in aluminum: First-principles calculations of structure and thermodynamics, *Phys. Rev. B* **69**, 144109 (2004).
- [45] R. Armiento and A. E. Mattsson, Functional designed to include surface effects in self-consistent density functional theory, *Phys. Rev. B* **72**, 085108 (2005).
- [46] G. Lu and E. Kaxiras, Hydrogen Embrittlement of Aluminum: The Crucial Role of Vacancies, *Phys. Rev. Lett.* **94**, 155501 (2005).
- [47] V. Jmerik, T. Shubina, A. Mizerov, K. Belyaev, A. Sakharov, M. Zamoryanskaya, A. Sitnikova, V. Davydov, P. Kop'ev, E. Lutsenko, N. V. Rzhetskii, A. V. Danilchik, G. P. Yablonskii, and S. V. Ivanov, AlGaN quantum well structures for deep-UV LEDs grown by plasma-assisted MBE using sub-monolayer digital-alloying technique, *J. Cryst. Growth* **311**, 2080 (2009).
- [48] Z. D. Popovic and M. J. Stott, Nonlinear, Self-Consistent Theory of Proton Screening in Metals Applied to Hydrogen in Al and Mg, *Phys. Rev. Lett.* **33**, 1164 (1974).
- [49] J.-C. Lian, H.-Y. Wu, W.-Q. Huang, W. Hu, and G.-F. Huang, Algorithm for generating irreducible site-occupancy configurations, *Phys. Rev. B* **102**, 134209 (2020).
- [50] P. Giannozzi, S. Baroni, N. Bonini, M. Calandra, R. Car, C. Cavazzoni, D. Ceresoli, G. L. Chiarotti, M. Cococcioni, I. Dabo, A. Dal Corso, S. de Gironcoli, S. Fabris, G. Fratesi, R. Gebauer, U. Gerstmann, C. Gougoussis, A. Kokalj, M. Lazzeri, L. Martin-Samos *et al.*, QUANTUM ESPRESSO: A modular and open-source software project for quantum simulations of materials, *J. Phys.: Condens. Matter* **21**, 395502 (2009).
- [51] P. Giannozzi, O. Andreussi, T. Brumme, O. Bunau, M. B. Nardelli, M. Calandra, R. Car, C. Cavazzoni, D. Ceresoli, M. Cococcioni, N. Colonna, I. Carnimeo, A. Dal Corso, S. de Gironcoli, P. Delugas, R. A. DiStasio Jr., A. Ferretti, A. Floris, G. Fratesi, G. Fugallo *et al.*, Advanced capabilities for materials modelling with Quantum ESPRESSO, *J. Phys.: Condens. Matter* **29**, 465901 (2017).
- [52] P. Giannozzi, O. Baseggio, P. Bonfà, D. Brunato, R. Car, I. Carnimeo, C. Cavazzoni, S. de Gironcoli, P. Delugas, F. Ferrari Ruffino, A. Ferretti, N. Marzari, I. Timrov, A. Urru, and S. Baroni, Quantum ESPRESSO toward the exascale, *J. Chem. Phys.* **152**, 154105 (2020).
- [53] M. Schlipf and F. Gygi, Optimization algorithm for the generation of ONCV pseudopotentials, *Comput. Phys. Commun.* **196**, 36 (2015).
- [54] A. Floris, A. Sanna, S. Massidda, and E. K. U. Gross, Two-band superconductivity in Pb from *ab initio* calculations, *Phys. Rev. B* **75**, 054508 (2007).
- [55] I. Errea, M. Calandra, and F. Mauri, First-Principles Theory of Anharmonicity and the Inverse Isotope Effect in Superconducting Palladium-Hydride Compounds, *Phys. Rev. Lett.* **111**, 177002 (2013).
- [56] I. Errea, M. Calandra, C. J. Pickard, J. Nelson, R. J. Needs, Y. Li, H. Liu, Y. Zhang, Y. Ma, and F. Mauri, High-Pressure Hydrogen Sulfide from First Principles: A Strongly Anharmonic Phonon-Mediated Superconductor, *Phys. Rev. Lett.* **114**, 157004 (2015).
- [57] I. Errea, F. Belli, L. Monacelli, A. Sanna, T. Koretsune, T. Tadano, R. Bianco, M. Calandra, R. Arita, F. Mauri, and J. A. Flores-Livas, Quantum crystal structure in the 250-kelvin superconducting lanthanum hydride, *Nature (London)* **578**, 66 (2020).
- [58] P. Hou, F. Belli, R. Bianco, and I. Errea, Strong anharmonic and quantum effects in $Pm\bar{3}n$ AlH₃ under high pressure: A first-principles study, *Phys. Rev. B* **103**, 134305 (2021).
- [59] M. T. Yin and M. L. Cohen, Microscopic Theory of the Phase Transformation and Lattice Dynamics of Si, *Phys. Rev. Lett.* **45**, 1004 (1980).
- [60] J. J. Rush, J. M. Rowe, and D. Richter, Direct determination of the anharmonic vibrational potential for H in Pd, *Z. Phys. B: Condens. Matter* **55**, 283 (1984).
- [61] S. Baroni, S. de Gironcoli, A. Dal Corso, and P. Giannozzi, Phonons and related crystal properties from density-functional perturbation theory, *Rev. Mod. Phys.* **73**, 515 (2001).
- [62] F. Giustino, M. L. Cohen, and S. G. Louie, Electron-phonon interaction using Wannier functions, *Phys. Rev. B* **76**, 165108 (2007).
- [63] S. Poncé, E. R. Margine, C. Verdi, and F. Giustino, EPW: Electron-phonon coupling, transport and superconducting properties using maximally localized Wannier functions, *Comput. Phys. Commun.* **209**, 116 (2016).
- [64] F. Giustino, Electron-phonon interactions from first principles, *Rev. Mod. Phys.* **89**, 015003 (2017).
- [65] G. Pizzi, V. Vitale, R. Arita, S. Blügel, F. Freimuth, G. Géranton, M. Gibertini, D. Gresch, C. Johnson, T. Koretsune, J. Ibañez-Azpiroz, H. Lee, J.-M. Lihm, D. Marchand, A. Marrazzo, Y. Mokrousov, J. I. Mustafa, Y. Nohara, Y. Nomura, L. Paulatto *et al.*, Wannier90 as a community code: New features and applications, *J. Phys.: Condens. Matter* **32**, 165902 (2020).
- [66] M. Gao, Z.-Y. Lu, and T. Xiang, Prediction of phonon-mediated high-temperature superconductivity in Li₃B₄C₂, *Phys. Rev. B* **91**, 045132 (2015).
- [67] A. Dal Corso, Pseudopotentials periodic table: From H to Pu, *Comput. Mater. Sci.* **95**, 337 (2014).
- [68] The Elk code, <https://elk.sourceforge.io/>.
- [69] S. Giaremis, P. Komninou, T. Karakostas, and J. Kioseoglou, *Ab initio* study of the electron-phonon coupling in ultrathin Al layers, *J. Low Temp. Phys.* **203**, 180 (2021).
- [70] E. R. Margine and F. Giustino, Anisotropic Migdal-Eliashberg theory using Wannier functions, *Phys. Rev. B* **87**, 024505 (2013).
- [71] B. Nedrud and D. Ginsberg, Localized modes of oscillation in hydrogen and deuterium doped lead, *Phys. B+C (Amsterdam)* **108**, 1175 (1981).
- [72] P. B. Allen and R. C. Dynes, Transition temperature of strongly-coupled superconductors reanalyzed, *Phys. Rev. B* **12**, 905 (1975).
- [73] Y. Takada, Mechanism of superconductivity in graphite-alkali metal intercalation compounds, *J. Phys. Soc. Jpn.* **51**, 63 (1982).
- [74] Y. Takada, Unified model for superconductivity in graphite intercalation compounds: Prediction of optimum T_c and suggestion for its realization, *J. Phys. Soc. Jpn.* **78**, 013703 (2009).

- [75] J. P. Carbotte, Properties of boson-exchange superconductors, *Rev. Mod. Phys.* **62**, 1027 (1990).
- [76] P. B. Allen and B. Mitrović, Theory of superconducting T_c , *Solid State Phys.* **37**, 1 (1983).
- [77] M. A. Biondi and M. P. Garfunkel, Measurement of the Temperature Variation of the Energy Gap in Superconducting Aluminum, *Phys. Rev. Lett.* **2**, 143 (1959).
- [78] D. H. Douglass, Direct Experimental Measurement of the Magnetic Field Dependence of the Superconducting Energy Gap of Aluminum, *Phys. Rev. Lett.* **7**, 14 (1961).
- [79] L. Testardi, J. Wernick, and W. Royer, Superconductivity with onset above 23° K in Nb-Ge sputtered films, *Solid State Commun.* **15**, 1 (1974).
- [80] J. Nagamatsu, N. Nakagawa, T. Muranaka, Y. Zenitani, and J. Akimitsu, Superconductivity at 39 K in magnesium diboride, *Nature (London)* **410**, 63 (2001).
- [81] J. Bardeen and M. Stephen, Free-Energy Difference Between Normal and Superconducting States, *Phys. Rev.* **136**, A1485 (1964).
- [82] H. J. Choi, M. L. Cohen, and S. G. Louie, Anisotropic Eliashberg theory of MgB_2 : T_c , isotope effects, superconducting energy gaps, quasiparticles, and specific heat, *Phys. C (Amsterdam)* **385**, 66 (2003).
- [83] J. Corsan and A. Cook, Electronic specific heat and superconducting properties of Nb-Ta alloys, *Phys. Lett. A* **28**, 500 (1969).